https://doi.org/10.5194/essd-2022-436
Preprint. Discussion started: 17 January 2023

A grid dataset of leaf age-dependent LAI seasonality product (Lad-LAI) over tropical and subtropical evergreen broadleaved forests

Xueqin Yang[1,2,3], Xiuzhi Chen[1,2,*], Jiashun Ren[1,4], Wenping Yuan[1,2], Liyang Liu[5], Juxiu Liu[6], Dexiang Chen[7], Yihua Xiao[7], Shengbiao Wu[8], Lei Fan[9], Xiaoai Dai[4], and Yongxian Su[3]

[1]Guangdong Province Key Laboratory for Climate Change and Natural Disaster Studies, School of Atmospheric Sciences, Sun Yat-sen University, Zhuhai 519082, China

[2]Southern Marine Science and Engineering Guangdong Laboratory (Zhuhai), Zhuhai 519082, China

[3]Key Lab of Guangdong for Utilization of Remote Sensing and Geographical Information System, Guangdong Open Laboratory of Geospatial Information Technology and Application, Guangzhou Institute of Geography, Guangdong Academy of Sciences, Guangzhou 510070, China

[4]College of Earth Sciences, Chengdu University of Technology, Chengdu 610000, China;

[5]Laboratoire des Sciences du Climat et de l'Environnement, IPSL, CEA-CNRS-UVSQ, Université Paris-Saclay, 91191 Gif sur Yvette, France

[6]Dinghushan Forest Ecosystem Research Station, South China Botanical Garden, Chinese Academy of Sciences, Guangzhou 510650, China;

[7]Pearl River Delta Forest Ecosystem Research Station, Research Institute of Tropical Forestry, Chinese Academy of Forestry, Guangzhou 510650, China;

[8]School of Biological Sciences, The University of Hong Kong, Pokfulam, Hong Kong

[9]Chongqing Jinfo Mountain Karst Ecosystem National Observation and Research Station, School of Geographical Sciences, Southwest University, Chongqing 400715, China

** Correspondence: Xiuzhi Chen (chenxzh73@mail.sysu.edu.cn)*

https://doi.org/10.5194/essd-2022-436
Preprint. Discussion started: 17 January 2023

Abstract

Quantification of large-scale leaf age-dependent leaf area index has been lacking in tropical and subtropical evergreen broadleaved forests (TEFs) despite the recognized importance of leaf age in influencing leaf photosynthetic capacity in this region. Here, we simplified the canopy leaves of TEFs into three age cohorts, i.e., young, mature and old one, with different photosynthesis capacity ($V_{c,max}$) and produced a first grid dataset of leaf age-dependent LAI product (**referred to as Lad-LAI**) over the continental scale from satellite observations of TROPOMI (the TROPOspheric Monitoring Instrument) sun-induced chlorophyll fluorescence (SIF) as a proxy of leaf photosynthesis. The seasonality of three LAI cohorts from the new Lad-LAI products agree well at the three sites (one in subtropical Asia and two in Amazon) with very fine collections of monthly LAI of young, mature and old leaves. Continental-scale comparisons with independent Moderate-resolution Imaging Spectroradiometer (MODIS) Enhanced Vegetation Index (EVI) products and 53 samples of *in situ* measurements of seasonal litterfall data also demonstrate the robustness of the LAI seasonality of the three leaf age cohorts. The spatial patterns clustered from the three LAI cohorts coincides with those clustered from climatic variables. And the young and mature LAI cohorts perform well in capturing a dry-season green-up of canopy leaves across the wet Amazonia areas where mean annual precipitation exceeds 2,000 mm yr^{-1}, consistent with previous satellite data analysis. The new Lad-LAI products are primed to diagnose the adaption of tropical and subtropical forest to climate change; and will also help improve the development of phenology modules in Earth System Models. The proposed satellite-based approaches can provide reference for mapping finer temporal and spatial resolution LAI products with different leaf age cohorts. The Lad-LAI products are available at https://doi.org/10.6084/m9.figshare.21700955.v2 (Yang et al., 2022).

1. Introduction

https://doi.org/10.5194/essd-2022-436
Preprint. Discussion started: 17 January 2023

Canopy phenology is the primary cause of photosynthetic seasonality (Chen et al., 2020; Wu et al., 2016) and thus largely regulates the seasonal carbon sinks (Beer et al., 2010; Aragao et al., 2014; Saatchi et al., 2011) in tropical and subtropical evergreen broadleaved forests (EBFs). However, the ecological connotations of canopy phenology in tropical and subtropical EBFs differ greatly from those in temperate and boreal forests, that is, the latter one is closely related to a critical plant trait — total leaf area index (LAI) that shows remarkable seasonal variations while the former one is rarely linked to the total LAI which shows marginally small seasonal changes (Wu et al., 2016; Chen et al., 2020). Due to the useless of total LAI as a proxy for tropical phenology, it remains less clear what is the most effective plant trait to represent the phenology seasonality in tropical and subtropical EBFs.

Recently, leaf age-dependent LAI is convergently shown by studies to well representation of canopy phenology in tropical and subtropical EBFs (Chen et al., 2020). Although there are less seasonal variations in the LAI of entire canopy, LAI of different leaf age classes (i.e., cohorts) show considerable seasonality (Wu et al., 2016). *In situ* measurements, even though spatially sparse, recorded an increase in LAI of young and mature leaves and conversely a decrease in LAI of old leaves as solar radiation enhances (Wu et al., 2016). The key point is that LAI of young and mature leaf cohorts dominate regulating the seasonal cycles of carbon fluxes (Albert et al., 2018; Doughty and Goulden, 2008a; Wu et al., 2016). It is because that the newly-flushed young leaves and maturing leaves show higher photosynthetic capacity than the old leaves being replaced (Xu et al., 2017), and thereby increase canopy photosynthesis by taking more advantage of surface radiation (Anber et al., 2015; Wu et al., 2017), even during the dry seasons (Manoli et al., 2018; Restrepo-Coupe et al., 2013; 2017; Saleska et al., 2003; 2016; Xu et al., 2015; Morton et al., 2014; Guan et al., 2015). This phenomenon has been well documented from eddy covariance data (Wu et al., 2016), biometric measurements of canopy foliage productivity (Doughty et al., 2015) and ESM model-derived LAI and gross primary production data (De Weirdt et al., 2012; Chen et al.,

https://doi.org/10.5194/essd-2022-436
Preprint. Discussion started: 17 January 2023

2020; Chen et al., 2021) in both humid- and dry-land tropical and subtropical EBFs. However, seasonal patterns of leaf age-dependent LAI are still unclear and are rarely studied at the continental scale. This vague notion \ imposes a challenge for accurately modeling continental-scale canopy photosynthesis seasonality in most land surface models (LSMs) due to their poor representation of the canopy phenology in tropical and subtropical EBF biomes (Restrepo-Coupe et al., 2017; Chen et al., 2021).

In this study, we aim to fill this gap by firstly mapping the seasonal LAI of three leaf age cohorts (i.e., young, mature and old leaves, denoted as LAI_{young}, LAI_{mature}, and LAI_{old}, respectively) to interpret the phenological seasonality in tropical and subtropical EBF biomes from 2001 to 2018. We simplified that canopy photosynthesis (i.e., gross primary production (GPP)) is composed of three parts that are produced from young, mature and old leaves, respectively. Based on this assumption, GPP is expressed as functions of the sum of the product of each LAI cohort (LAI_{young}, LAI_{mature}, and LAI_{old}) and corresponding net CO_2 assimilation rate (An_{young}, An_{mature}, and An_{old}), which is calculated by the widely used Farquhar-von Caemmerer-Berry (FvCB) leaf photochemistry model (Farquhar et al., 1980). And the grid GPP maps are linearly derived from an arguably better proxy — TROPOMI (the TROPOspheric Monitoring Instrument) Solar-Induced Fluorescence (SIF) calibrated by eddy covariance GPP data.

To decompose the three LAI cohorts from **Equation 1**, we hypothesized that the adjacent four cells in the grid map exhibit consistent magnitude and seasonality of GPP, LAI_{young}, LAI_{mature}, and LAI_{old}. Then, we applied **Equation 1** to each of the four selected cells and combined the four equations to derive the three LAI cohorts using a linear least-squares with constrained method. *In situ* measurements of seasonal LAI_{young}, LAI_{mature}, and LAI_{old} in two Amazonian sites and subtropical Asian sites (blue pentangles in **Fig. 1, Table S1**) are used to directly validate the simulating results. To prove the robustness of the products over a large spatial coverage, the seasonal LAI cohorts of young and mature leaves are evaluated against the enhanced vegetation index (EVI) product, which is considered as a proxy for leaf area changes of photosynthetic

https://doi.org/10.5194/essd-2022-436
Preprint. Discussion started: 17 January 2023

effective leaves (Saatchi, et al., 2015; Wu et al., 2016). Additionally, the LAI cohorts of old leaves are compared with the phase of litterfall mass from 53 *in situ* sites (black circles in **Fig. 1**) spanning tropical and subtropical EBF regions. This new dataset of three LAI cohorts provides new insights into tropical and subtropical phenology with more details of sub-canopy level of leaf seasonality in different leaf age cohorts and will be helpful for developing accurate tropical phenology model in ESMs.

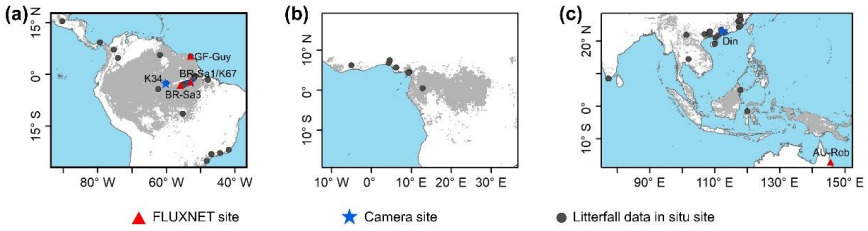

Figure 1. Study areas over tropical and sub-tropical for evergreen broadleaves forests. Red triangles: four sites of EC-observed GPP seasonality. Blue pentangles: observation sites of three LAI cohort seasonality. Black circles: observation sites of litterfall seasonality.

2. Methodology

2.1 Decomposing LAI cohorts (young, mature and old) from SIF-derived GPP

Figure 2 illustrates the overall framework used to generate leaf age-dependent LAI seasonality product (Lad-LAI). The majority of the tropical and subtropical EBFs retain leaves year-round and their total LAI shows marginally small seasonal changes (Wu et al., 2016). Therefore, previous modelling studies have assumed a constant value for the total LAI in tropical and subtropical EBFs (Cramer et al., 2001; Arora and Boer, 2005). In this study, we follow above previous studies to assume a total constant value (total LAI= 7) of total LAI in tropical and subtropical EBFs. We grouped the canopy leaves of tropical and subtropical EBFs into three leaf age cohorts, i.e., young, mature and old leaves, respectively. Then, the total GPP is the sum of those produced by the young, mature and old leaves, respectively. According to the Farquhar-von Caemmerer-Berry

https://doi.org/10.5194/essd-2022-436
Preprint. Discussion started: 17 January 2023

(FvCB) leaf photochemistry model (Farquhar et al., 1980), GPP can be expressed as function of the sum of the products of each LAI cohort (LAI_{young}, LAI_{mature}, and LAI_{old}) and corresponding net CO_2 assimilation rate (An_{young}, An_{mature}, and An_{old}) (**Equantion 1**).

$$LAI_{young} \times An_{young} + LAI_{mature} \times An_{mature} + LAI_{old} \times An_{old} = GPP \qquad (1)$$

where LAI_{young}, LAI_{mature} and LAI_{old} are the leaf area index cohorts; An_{young}, An_{mature} and An_{old} are the net rate of CO_2 assimilation dependent on three leaf age classes; GPP is canopy total gross primary production. The sum of LAI_{young}, LAI_{mature} and LAI_{old} is set as a constant, equaling to 7 according to Chen et al. (2020).

The GPP is derived from SIF (denoted as RTSIF-derived GPP) using a linear regression model (see sect. 2.2) based on the relationship between RTSIF and EC-observed GPP from 4 sites (**Table S2**). The An_{young}, An_{mature} and An_{old} are calculated according to the FvCB biochemical model (Farquhar et al., 1980; Bernacchi et al., 2003) (see sect. 2.3). As there are still three unknow variables to be solved in equation 1 (LAI_{young}, LAI_{mature} and LAI_{old}), we hypothesized that the adjacent four pixels exhibit homogenous EBFs and consistent leaf demography and canopy photosynthesis. Then, we used the data from adjacent four pixels to solve the LAI_{young}, LAI_{mature} and LAI_{old} from GPP based on **Equation 1** sing a linear least-squares with constrained method. The inputs grid datasets (i.e. SIF-derived GPP, T_{air}, VPD and SW, **Table S3**) in **Fig. 2** are sampled at 0.125-degree spatial resolution; while the output maps of LAI_{young}, LAI_{mature}, and LAI_{old} are at 0.25-degree spatial resolution. Therefore, the output maps of LAI_{young}, LAI_{mature}, and LAI_{old} are at a 0.25-degree spatial resolution. We used Python version 3.7 (Python Software Foundation, http://www.python.org) and matlab R2019b for all our analyses.

https://doi.org/10.5194/essd-2022-436
Preprint. Discussion started: 17 January 2023

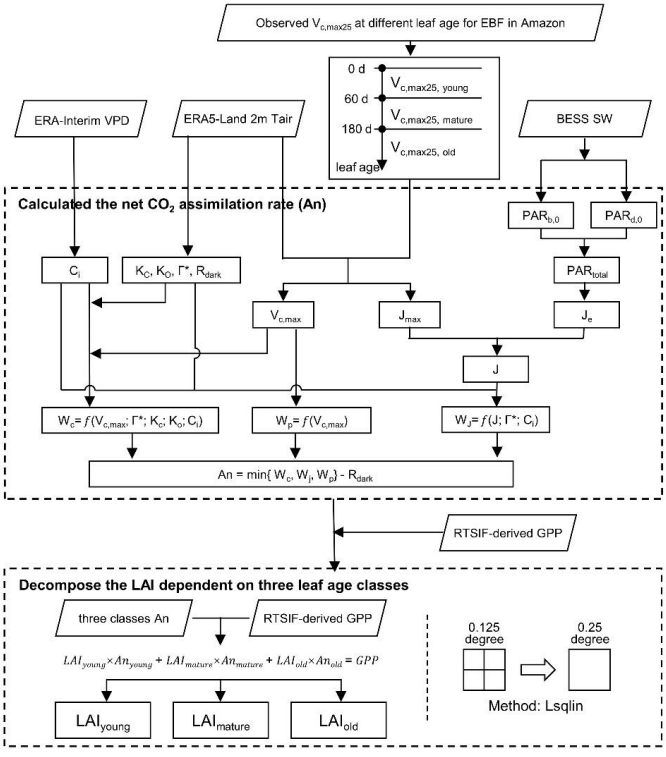

Figure 2. The workflow for mapping Lad-LAI using the Lsqlin method. Lsqlin is the abbreviation of Linear least-squares solver with bounds or linear constraints. All the abbreviations are described in supplementary **Tables S4**.

2.2 Calculating the GPP from TROPOMI SIF (RTSIF-derived GPP)

Satellite-retrieved solar-induced chlorophyll fluorescence (SIF) is a widely used proxy for canopy photosynthesis (Yang et al., 2015; Dechant et al., 2020). Here, we used a long-term reconstructed TROPOMI SIF dataset (RTSIF) (Chen et al., 2022) to estimate GPP seasonality. Previous analyses show that RTSIF is strongly linearly correlated to eddy covariance (EC) GPP and used 15.343 as a transformation coefficient to covert RTSIF to GPP (Fig. 8a in Chen et al., 2022). In this study, we collected GPP data at 4 EC sites from the FLUXNET 2015 Tier 1 dataset (**Table S2**; Pastorello et al.,

https://doi.org/10.5194/essd-2022-436
Preprint. Discussion started: 17 January 2023

2020) and examined the relationship between RTSIF-derived GPP and EC GPP (**Fig. 3**). Results confirmed the robustness of estimating the GPP seasonality using RTSIF-derived GPP (R^2>0.90). Despite potential overestimation (**Fig. 3 b**) or underestimation (**Fig. 3 h**) of the magnitudes, RTSIF-derived GPP mostly captures the seasonality of the EC GPP at all the 4 sites (d_{phase} < 0.26).

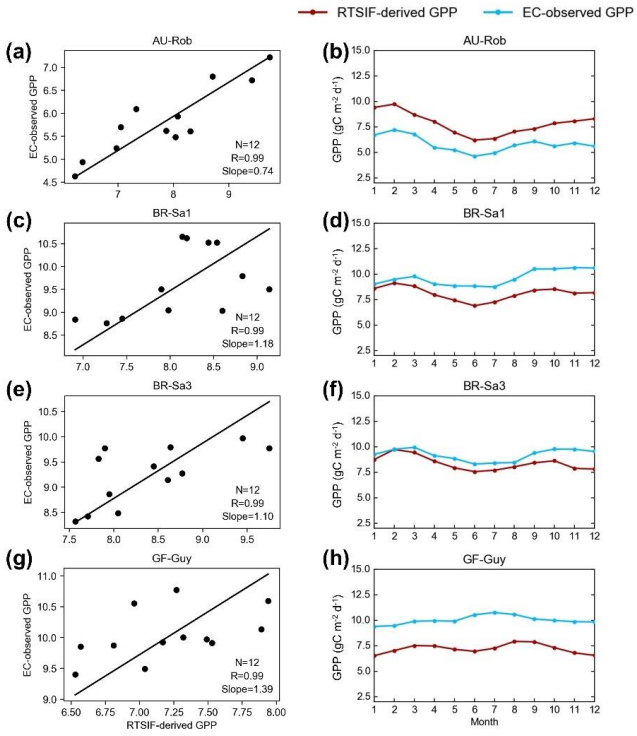

Figure 3. Comparisons between monthly RTSIF-derived GPP (red) and EC-observed GPP (blue). (a-b) Au-Rob, (c-d) BR-Sa1, (e-f) BR-Sa3, and (g-h) GF-Guy. The regression is forced to pass the origin.

2.3 Calculating the net rate of CO_2 assimilation (An)

We calculated the net CO_2 assimilation (An) according to the FvCB biochemical model (Farquhar et al., 1980). In this model, the parameter An is calculated as the minimum of Rubisco (W_c), RuBP regeneration (W_j) and TPU (W_p), respectively, minus dark respiration (R_{dark}) (Bernacchi et al., 2013). The formulas for calculating An, W_c,

https://doi.org/10.5194/essd-2022-436
Preprint. Discussion started: 17 January 2023

W_j, W_p, R_{dark} and corresponding intermediate variables are listed in **Tables S4**.

Calculation of W_c. W_c is expressed as a function of internal CO_2 concentration (c_i), Michaelis-Menton constant for carboxylase (K_c), Michaelis-Menton constant for oxygenase (K_o), CO_2 compensation point (Γ^*) and maximum carboxylation rate ($V_{c,max}$) (**Table S4-part1**) (Lin et al., 2015; Bernacchi et al., 2013; Ryu et al., 2011; Medlyn et al., 2011; June et al., 2004; Farquhar et al., 1980). The K_c, K_o, Γ^* and $V_{c,max}$ are temperature-dependent variables. Thus, we used **Equation 2** to calculate their values at T_k by converting from those at 25°C. Then, we used the Medlyn's stomatal conductance model (Medlyn et al., 2011) to estimate internal CO_2 concentration (c_i) (**Equation 3**), which is expressed as a function of vapor pressure deficit (VPD) rather than relative humidity (Lin et al., 2015). The method of $V_{c,max}$ calculating for each LAI cohort is introduced in sect. 2.4. The formulas for calculating corresponding intermediate parameters are presented in **Table S4 -part2**.

$$Para = Para_{25} \times exp\left(\frac{(T_k - 298.15) \times \Delta H_{para}}{R \times T_k \times 298.15}\right) \quad (2)$$

where Para denotes a correction factor arising from the temperature dependence of $V_{c,max}$; $Para_{25}$ are values of the temperature-dependent parameters (K_c, K_o, Γ^* and $V_{c,max}$) at the temperature 25°C; T_k denotes temperature in Kelvin; ΔH_{para} is activation energy for temperature dependence; R is universal gas constant.

$$c_i = c_a \times \left(1 - \frac{1}{1.6 \times \left(1 + \frac{g_1}{\sqrt{VPD}}\right)}\right) \quad (3)$$

where c_a is atmospheric CO_2 concentration, 380 ppm; VPD is calculated from air temperature and dew point temperature of the global ERA-Interim reanalysis dataset (Dee et al., 2011) using the method of Yuan et al. (2019). The calculation formula of VPD is described in supplementary files. In this study, we used the value of 3.77 for the stomatal slope (g_1) in the stomatal conductance model according to Lin et al. (2015).

Calculation of W_p. W_p is calculated as the function of $V_{c,max}$, which are given different values for different LAI cohorts based on multiple *in situ* observations (sect. 2.4).

https://doi.org/10.5194/essd-2022-436
Preprint. Discussion started: 17 January 2023

Calculation of W_j. W_j is calculated from $V_{c,max}$, c_i and the rate of electrons through the thylakoid membrane (J) (Bernacchi et al., 2013). The parameter J is calculated from maximum electron transport rate (J_{max}) and the rate of whole electron transport provided by light (J_e) (Bernacchi et al., 2013). J_{max} is expressed as a temperature dependence function of maximum electron transport rate ($J_{max,25}$) at 25℃ and temperature (T_{air}) and J_e is expressed as a function of total PAR absorbed by canopy (PAR_{total}), which is the sum of active radiation in beam ($PAR_{b,0}$) and diffuse ($PAR_{d,0}$) light firstly (Weiss et al., 1985), which are calculated from downward short wave radiation (SW) (Zhang et al., 2014). The formula for PAR_{total} is given in **Equation 4** and formulas for other intermediate parameters 4 (i.e., $PAR_{b,0}$, $PAR_{d,0}$, ρ_{cb}, ρ_{cd}, k'_b, k'_d, and CI) are listed in **Table S4-part3** and **Table S4-part4**.

$$PAR_{total} = (1-\rho_{cb}) \times PAR_{b,0} \times \left(1 - exp(-k'_b \times CI \times LAI_{total})\right) + (1-\rho_{cd}) \times PAR_{d,0} \times \left(1 - exp(-k'_d \times CI \times LAI_{total})\right) \quad (4)$$

where PAR_{total} is total PAR absorbed by canopy; $PAR_{b,0}$ is the active radiation; $PAR_{d,0}$ is diffuse radiation; LAI_{total} is a total LAI and here we used a constant value of 7 according to Chen et al. (2020).

2.4 Classifying three LAI cohorts with different $V_{c,max}$

In this study, we collected *in situ* samples of $V_{c,max25}$ data against different leaf age across tropical and subtropical EBFs from previous publications (Keller et al., 2001; Araújo, 2002). Mature leaves (leaf age: 70-160 days) show highest $V_{c,max25}$ than those of new flushed leaves (leaf age: <60 days) and old leaves(leaf age: >200 days) as Menezes et al. (2022). Therefore, in this study, we also classified the canopy leaves into three cohorts: young (leaf age: <2 months), mature (leaf age: 3-5 months) and old cohorts (leaf age: >6 months) as Wu et al. (2016). The $V_{c,max25}$ for young, mature and old cohorts are set as 60, 40 and 20 μmol m^{-2} s^{-1}, respectively, according to previous ground-based observations (Keller et al., 2001; Araújo, 2002).

https://doi.org/10.5194/essd-2022-436
Preprint. Discussion started: 17 January 2023

2.5 Ground-based observations for LAI cohort validations

At present, there are only several studies that have decomposed the total LAI into different leaf age cohorts. Thus, only three sites with observation of LAI_{young}, LAI_{mature} and LAI_{old} are used for validating the corresponding simulated LAI cohorts. Two sites (K67 and K34) are at Amazon (Wu et al., 2016). The mean monthly LAI cohorts were calculated from top-of-canopy images of a Tetracam Agricultural Digital Camera (Wu et al., 2016). The camera-inferred LAIs were classified into three cohorts based on different leaf ages: young (<2 months); mature (3–5months); old (>6 months). Detailed information on camera data processing is given by Wu et al. (2016).

Another site is at Dinghushan station in subtropical China. The hourly top - of - canopy images of trees are observed by an RGB camera. This study classified the canopy leaves into young, mature and old age cohorts based on the green-color band, as the brightness of different leaf age leaves in the same band differ greatly. Raster density slicing is a useful classification method for detecting the attributes of various ground objects (Kartikeyan et al., 1998). Therefore, we set three brightness thresholds to divide young (blue), mature (green), old (yellow) leaves and background (gray) for the same canopy extent in each month (**Fig. 4**). This analysis is conducted in ENVI5.3 software.

https://doi.org/10.5194/essd-2022-436
Preprint. Discussion started: 17 January 2023

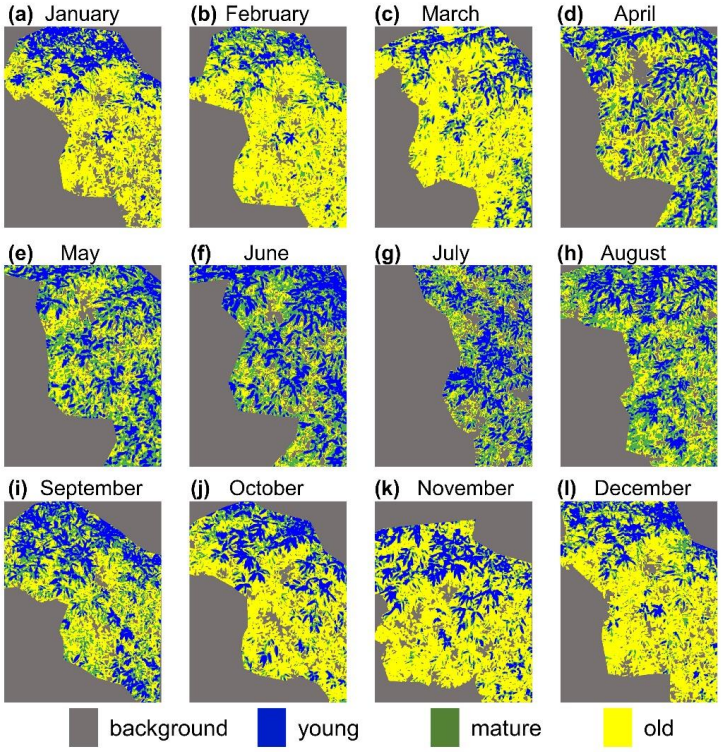

Figure 4. Classifications of canopy leaves into young, mature and old age cohorts in Dinghushan station. The boundaries of the imageries are those of the tree canopies that vary between months.

2.6 Evaluating the LAI of young and mature leaf age cohorts using satellite-based EVI

To evaluate the LAI seasonality of photosynthesis-effective leaves, i.e. young and mature leaves, this study used satellite-based MODIS Enhanced Vegetation Index (EVI) from independent sensors (Huete et al., 2002; Lopes et al., 2016; Kobayashi, et al., 2018) as a remotely sensed proxies alternatives of effective leaf area changes and new leaf flush, i.e., $LAI_{young+mature}$ (Wu et al., 2016; Saatchi, et al., 2015). To compare the seasonality of $LAI_{young+mature}$ with those of EVI, we calculate MSD and their three components—d_{bias}, which denotes the differences about absolute value, d_{var}, which denotes the differences of seasonal fluctuations, and d_{phase}, which denotes the

https://doi.org/10.5194/essd-2022-436
Preprint. Discussion started: 17 January 2023

differences of peak phase to evaluate this consistence, comprehensively (see Methodology 2.8 section).

Additionally, we compared the spatial patterns of the wet- minus dry-season differences (Δ) between observed and simulated variables, following the work of Guan, et al. (2015). To determine the wet and dry seasons in each grid cell, we defined a month as dry one when its monthly average precipitation was smaller than the potential evapotranspiration (PET) computed using the method of Maes et al. (2019); other months are classified as wet ones. The wet- minus dry-season $LAI_{young+mature}$ (denoted as $\Delta LAI_{young+mature}$) was calculated for each grid cell as the wet-season average $LAI_{young+mature}$ value minus the dry-season average value of $LAI_{young+mature}$.

2.7 Evaluating the LAI of old leaf age cohorts using ground-based litterfall

Litterfall is closely related to the seasonal dynamics of old leaves, i.e. LAI_{old} (Chen et al., 2020; Yang et al., 2021). Previous analyses indicated that, in general, a sharping decrease in LAI_{old} correspond to a peak in litterfall (Pastorello et al., 2020; Midoko Iponga et al., 2019; Ndakara, 2011; Barlow et al., 2007; Dantas and Phillipson, 1989). Based on this relationship between litterfall and LAI_{old}, we compare the time of seasonal litterfall peak with the time of sharpest negative slopes of LAI_{old}, to indirectly evaluate the LAI_{old} seasonality. To accurately detect the onset date of old leaves shedding and the day of litterfall peak, we used a least-square regression analysis method developed by Piao et al. (2006) to smoothen LAI_{old} and litterfall seasonal curves. The sixth-degree polynomial function (n=6) is applicable to the regression (**Equation 5**).

$$LAI_{old} = a_0 + a_1x + a_2x^2 + a_3x^3 + a_4x^4 + a_5x^5 + a_6x^6 \qquad (5)$$

where x is the day of a year.

Then, we identified the period of sharpest decrease in LAI_{old} as the beginning of leaves shedding season. For this purpose, we firstly calculated the slope of LAI_{old} curve, denoted as $LAI_{old,\ ratio}$ (**Equation 6**), from the series of consecutive 1-month periods

https://doi.org/10.5194/essd-2022-436
Preprint. Discussion started: 17 January 2023

and detected the time t with the maximum $LAI_{old,\ ratio}$, and then used the corresponding $LAI_{old(t)}$ as the LAI_{old} threshold for the onset date of old leaves shedding.

$$LAI_{old,ratio(t)} = \left(LAI_{old(t+1)} - LAI_{old(t)}\right)/\left(LAI_{old(t)}\right) \quad (6)$$

Then, we determined the onset dates of old leaves shedding for each litterfall site, using the polynomial regression results and the LAI_{old} thresholds calculated before, to compare with the day of litterfall peak (see in sect. 3.4). In this study, we collected 53 samples of monthly litterfall data across tropical and subtropical EBFs from globally published articles, and averaged multiyear data to the monthly mean data to compare with the seasonality of LAI_{old}. The geographical positions of 53 field observations were shown in **Fig. 1** (black circles). The seasonality of LAI (LAI_{young}, LAI_{mature}, LAI_{old}), litterfall mass, photosynthesis proxies (EVI, RTSIF-derived GPP) and climate proxies (T_{air}, VPD, SW) at these field are shown in **Fig. S1**. Litterfall datasets are listed in **Table S5**.

2.8 Evaluation Metrics

Two metrics were chosen to evaluate the seasonality of Lad-LAI against the that of other proxies: the Kobayashi decomposition of the Mean Square Difference between model and observation (Kobayashi and Salam, 2000) and the Pearson correlation coefficient (Pearson, 1896) for gridded fields.

Mean square deviation (MSD). The mean squared deviation (MSD) is given by Kobayashi and Salam (2000):

$$MSD = \frac{1}{n}\sum_{i=1}^{n}(x_i - y_i)^2 \quad (7)$$

$$SB = (\bar{x} - \bar{y})^2 \quad (8)$$

$$SD_s = \sqrt{\frac{1}{n}\sum_{i=1}^{n}(x_i - \bar{x})^2} \quad (9)$$

$$SD_m = \sqrt{\frac{1}{n}\sum_{i=1}^{n}(y_i - \bar{y})^2} \quad (10)$$

$$SDSD = (SD_s - SD_m)^2 \quad (11)$$

$$LCS = 2SD_sSD_m(1 - r) \quad (12)$$

https://doi.org/10.5194/essd-2022-436
Preprint. Discussion started: 17 January 2023

where mean squared deviation is the square of RMSD; i.e., MSD = $RMSD^2$.The lower the value of MSD, the closer the simulation is to the measurement. MSD can be decomposed into the sum of three components: the squared bias (d_{bias}), d_{bias}=SB; the squared difference between standard deviations (variance-related difference, d_{var}), d_{var}=SDSD; and the lack of correlation weighted by the standard deviations (phase-related difference, d_{phase}), d_{phase}=LCS; r indicates the correlation coefficient between x and y.

Pearson correlation coefficient (R). The Pearson correlation coefficient is a measure of linear correlation between two variables (Merkl and Waack, 2009). The correlation coefficient between X and Y is as:

$$\rho_{X,Y} = \frac{cov(X,Y)}{\sigma_X \sigma_Y} = \frac{E\big((X-\mu_X)(Y-\mu_Y)\big)}{\sigma_X \sigma_Y} \quad (13)$$

3. Results

3.1 Comparison of LAI cohort seasonality with sparse site observations

Despite very few site observations of LAI_{young}, LAI_{mature}, and LAI_{old} over TEFs, the leaf age-dependent LAI seasonality product agrees well with these camera - based measurements of LAI_{young}, LAI_{mature}, and LAI_{old} at K67, K34 sites in Amazon and Dingshuan site in China. The LAI seasonality of mature and old classes from the new Lad-LAI products agree well at these sites with very fine collections of monthly LAI of mature (R^2_{K67}=0.40, R^2_{K34}=0.81, R^2_{Din}=0.90; MSD_{K67}=1.55, MSD_{K34}=1.12, MSD_{Din}=6.33) and old leaves (R^2_{K67}=0.02, R^2_{K34}=0.40, R^2_{Din}=0.92; MSD_{K67}=0.87, MSD_{K34}=0.30, MSD_{Din}=15.57). However, the seasonality of LAI from young leaves performs a little poor in comparison with mature and old leaves (R^2_{K67}=0.24, R^2_{K34}=0.02, R^2_{Din}=0.48; MSD_{K67}=0.87, MSD_{K34}=0.65, MSD_{Din}=1.07). It is because that the trade-off between the phenology of mature and old leaves mainly control the seasonality of canopy photosynthesis. It is interesting to note that the canopy leaf phenology of TEFs at these sites differ greatly. At K67 and K34 sites, both *in situ* and simulated LAI_{young} and LAI_{mature} decrease at early wet season around February and

https://doi.org/10.5194/essd-2022-436
Preprint. Discussion started: 17 January 2023

convert to increase at early wet season around June (**Fig. 5 a-d**). On the contrary, at Dinghushan sites, LAI_{young} and LAI_{mature} increase during the wet season and peak with largest rainfall at June or July (**Fig. 5 e and f**). There is a reverse pattern for LAI_{old} seasonality compared to LAI_{mature} for all the three sites.

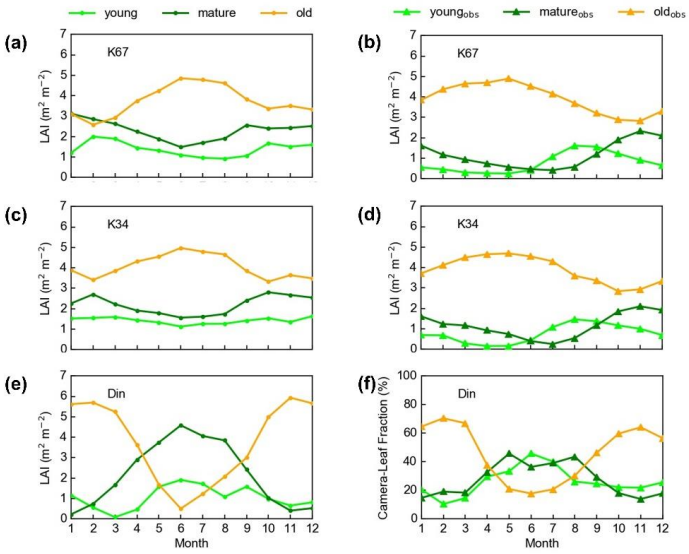

Figure 5. Seasonality of simulated LAI_{young}, LAI_{mature}, and LAI_{old} in comparison with observed data at Amazonian K67, K34 sites and Asian Dinghushan site.

3.2 Comparison of patterns of grid LAI cohort seasonality with previous climatic and phenological patterns

The *in situ* measurements of LAI_{young}, LAI_{mature}, and LAI_{old} suggest diverse patterns of Lad-LAI seasonality over the TEFs; while the sparse coverage of these site measurements limit a comprehensive and direct evaluation of leaf age-dependent LAI seasonality product. To continue in-depth sub-regional evaluations of the grid Lad-LAI seasonality product, we further conduct spatial clustering analyses of LAI_{young}, LAI_{mature}, and LAI_{old} using the *K*-means analysis method (see methods).

Surprisingly, the spatial clustering patterns of Lad-LAI product derived from satellite-based vegetative signals (**Fig. 6 g-i**) coincide well with those clustered from

https://doi.org/10.5194/essd-2022-436
Preprint. Discussion started: 17 January 2023

in-dependent climatic variables (rainfall and radiation etc.) (**Fig. 6 a-c**) (see methods). These patterns are also similar as those of the climate-phenology rhythms mapped by (Yang et al., 2021), which suggest different correlations of litterfall seasonality with canopy phenology between different climate-phenology rhythms.

In central (sub-region s2) and south (sub-region s3) Amazon (**Fig. 6 g**), the seasonality of LAI_{young}, LAI_{mature}, and LAI_{old} (**Fig. 7 b and c**) are similar as those of BR-Sa1 and BR-Sa3 sites. And in subtropical Asia (sub-region s6) (**Fig. 6 i**), the seasonality of three LAI cohorts (**Fig. 7 f**) are similar as those of Dinghushan sites. The remaining 4 sub-regions (sub-regions s1, s4, s5, s7) are all located nearby the equator. The magnitudes of seasonal changes in LAI cohorts are smaller than those in sub-regions s2, s3 and s6 away from the equator. It is worth noting that for these sub-regions around the equator there is a bimodal seasonality pattern for LAI_{mature}, with the first peak in around March and the second peak in around August (**Fig. 7 a, d, e and g**). This is consistent with the findings of Li et al. (2021) that showed tropical and subtropical TEFs changed from a unimodal phenology at higher-latitudes to a bimodal phenology at lower-latitudes.

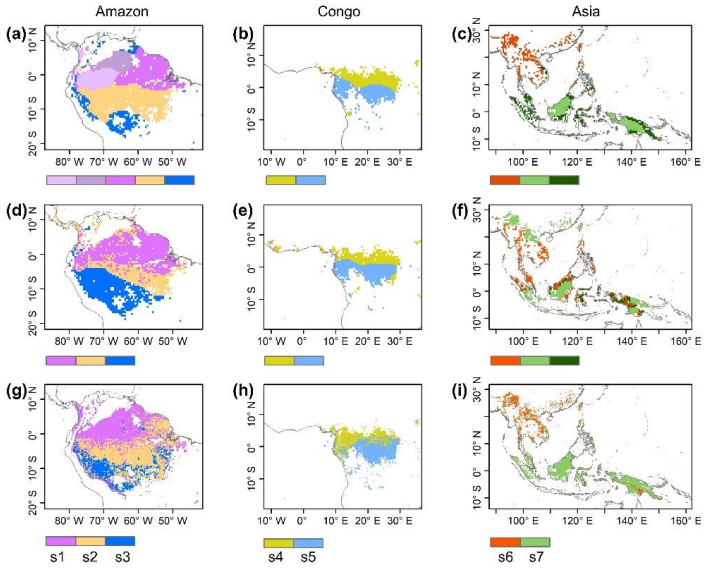

Figure 6. Comparison of sub-regions of Lad-LAI products (plots g-i) with those of

https://doi.org/10.5194/essd-2022-436
Preprint. Discussion started: 17 January 2023

climatic factors classified by the *K*-means clustering analysis (plots a-c) (Chen et al., 2019) and those of the three climate-phenology regimes (plots d-f) developed by Yang et al. (2021).

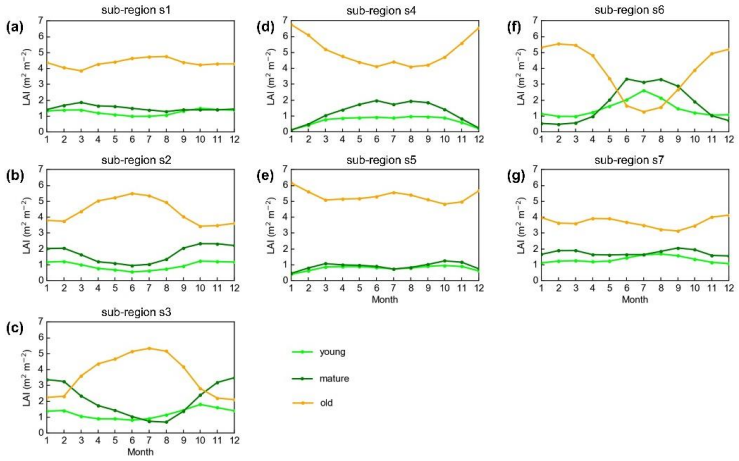

Figure 7. Seasonality of simulated LAI_{young}, LAI_{mature}, and LAI_{old} in sub-regions classified by the *K*-means clustering analysis.

3.3 Sub-regional evaluations of grid $LAI_{young+mature}$ seasonality using satellite-based EVI products

The grid dataset of $LAI_{young+mature}$ seasonality was indirectly evaluated using the satellite-based EVI products (Wang et al., 2017; De Moura et al., 2017; Xiao et al., 2005; Wu et al., 2018), as the Enhanced Vegetation Index (EVI) can be considered as a proxy for leaf area change of those leaves with high photosynthesis efficiency (Huete et al., 2006; Lopes et al., 2016; Wu et al., 2018). The linear correlation and MSD decompositions (see methods) between simulated and satellite-based EVI are displayed in **Fig. 8**. Overall, the seasonal $LAI_{young+mature}$ in 76.79% of the TEFs is well correlated with satellite-based EVI ($R^2 > 0.40$) (**Fig. 8 a-c**). The MSD is smaller than 0.1 in 90.59% of the TEFs over the whole tropical and subtropical region (**Fig. 8 d-f**). Statistics in the 7 clustered sub-regions show that the seasonal $LAI_{young+mature}$ of Lad-LAI data mostly

https://doi.org/10.5194/essd-2022-436
Preprint. Discussion started: 17 January 2023

correlate better with seasonal EVI in high-latitude areas (sub-region s2: R=0.66, sub-region s3: R=0.75, sub-region s6: R=0.71) than those in low latitudes (sub-region s1: R=0.44, sub-region s5: R=0.63, sub-region s7: R=0.40) except for sub-region s4 (R=0.76) (**Fig. 9**). The MSD components also confirm the better performance of $LAI_{young+mature}$ seasonality in high-latitude areas (sub-region s2:d_{bias}=0.010, d_{var}=0.001, d_{phase}=0.029; sub-region s3: d_{bias}=0.008, d_{var}=0.002, d_{phase}=0.028; sub-region s6: d_{bias}=0.013, d_{var}=0.005, d_{phase}=0.033) than in low-latitude areas near the Equator (sub-region s1: d_{bias}=0.022, d_{var}=0.002, d_{phase}=0.041; sub-region s4: d_{bias}=0.022, d_{var}=0.001, d_{phase}=0.025; sub-region s5: d_{bias}=0.022, d_{var}=0.001, d_{phase}=0.029; sub-region s7: d_{bias}=0.040, d_{var}=0.002, d_{phase}=0.043) (**Fig. 10**).

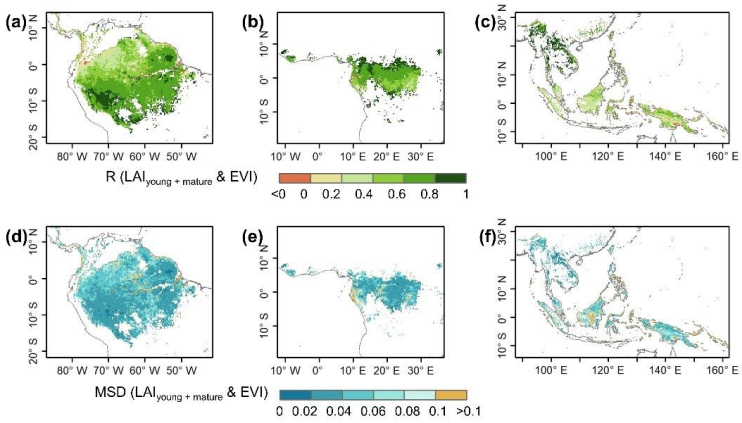

Figure 8. Pearson correlation coefficient (R) and Mean squared deviation (MSD) between seasonality of simulated $LAI_{young+mature}$ and MODIS Enhanced Vegetation Index (EVI).

https://doi.org/10.5194/essd-2022-436
Preprint. Discussion started: 17 January 2023

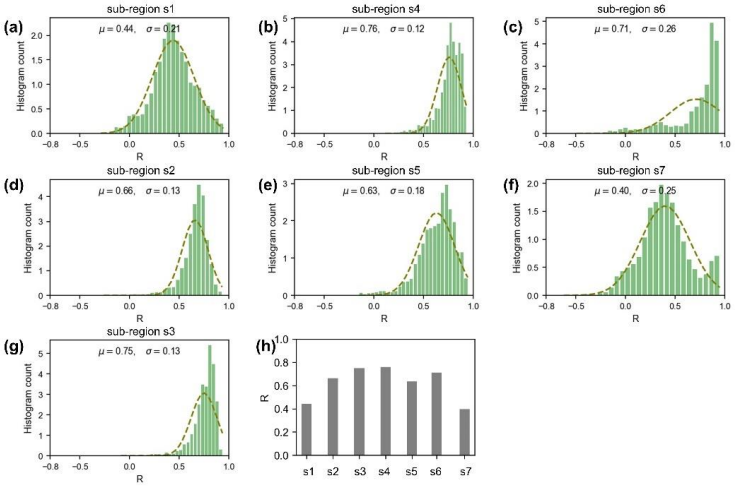

Figure 9. Statistics of the Pearson correlation coefficient (R) between seasonality of simulated $LAI_{young+mature}$ and MODIS Enhanced Vegetation Index (EVI) in the 7 clustered sub-regions. (a-g): the histogram of R; (h): mean of R in each sub-region

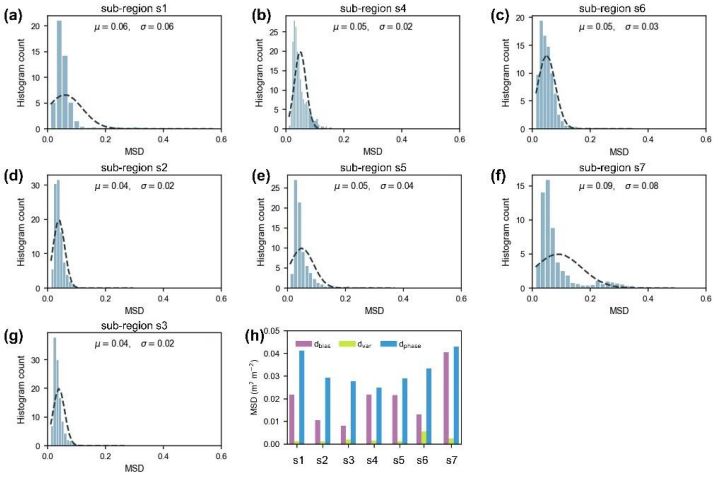

Figure 10. Statistics of the Mean squared deviation (MSD) between seasonality of simulated $LAI_{young+mature}$ and MODIS Enhanced Vegetation Index (EVI) in the 7 clustered sub-regions. (a-g): the histogram of MSD; (h): mean of MSD in each sub-region.

https://doi.org/10.5194/essd-2022-436
Preprint. Discussion started: 17 January 2023

Additionally, previous studies indicated large-scale dry-season green-up area over tropical and subtropical region (i.e., Guan et al., 2015, Tang et al., 2017, Myneny et al., 2007) where MAP exceeds 2,000 mm yr^{-1}. Here, we calculated the differences (Δ) between wet- and dry-season $LAI_{young+mature}$ (i.e., LAI_{young}+ LAI_{mature}), to test whether the Lad-LAI can capture this green-up spatial pattern. Spatial patterns of $\Delta LAI_{young+mature}$ (**Fig. 11**) were similar to those developed by (Guan et al., 2015), with higher $LAI_{young+mature}$ during the dry season (blue area) in large areas north of the Equator. This indicates an emergence of new leaf flush and increase of mature leaves, resulting the canopy "green-up" phenomenon observed by previous satellite-based signals. It is interesting to note that the total areas (blue regions in **Fig. 11**) of this dry-season green up shown by $LAI_{young+mature}$ is smaller than those shown by SIF signals that almost everywhere north of the Equator. That is because that new and mature leaves show quite a higher photosynthetic capacity than old leaves. A slight or moderate "green-up" in new and mature leaves (i.e., increase in $LAI_{young+mature}$) would boost strong increase in photosynthesis, inducing significant "green-up" shown by photosynthesis-related signals, e.g. SIF data. Therefore, using photosynthesis proxies likely overestimate the areas with "green-up" of new leaves during the dry seasons in the real world.

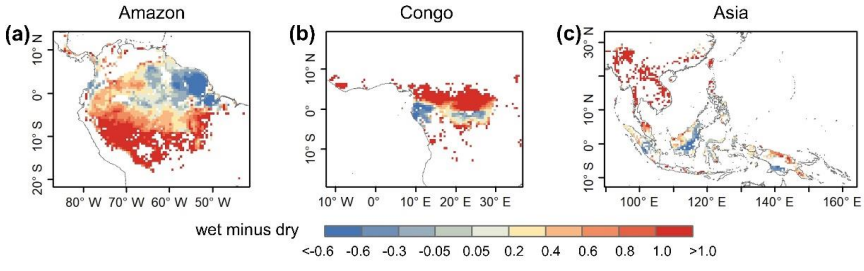

Figure 11. Spatial pattern of dry-season green-up using wet-season $LAI_{young+mature}$ minus dry-season $LAI_{young+mature}$.

https://doi.org/10.5194/essd-2022-436
Preprint. Discussion started: 17 January 2023

3.4 Sub-regional evaluations of grid LAI_{old} seasonality using site-based litterfall observations

The seasonal patterns of LAI_{old} were evaluated indirectly using site-based seasonal litterfall observations (black circles in **Fig. 1**). As there are 53 sites in total over the tropical and subtropical EBFs, we selected 9 specific sites for examples with different patterns of litterfall seasonality and LAI_{old} seasonality, to illustrate the analyses results. **Fig. 12 a-i** illustrate the days when there is a sharping decrease in monthly LAI_{old}, which are closely to monthly litterfall peak. The days when LAI_{old} decreases sharpest (Day_{LAIold}) agree well with the days when their monthly litterfall peaks ($Day_{litterfall}$) (**Fig. 12 j**), mostly distributed near the diagonal lines (R^2=0.90). This indirectly demonstrate the robustness of the LAI_{old} seasonality of the Lad-LAI product.

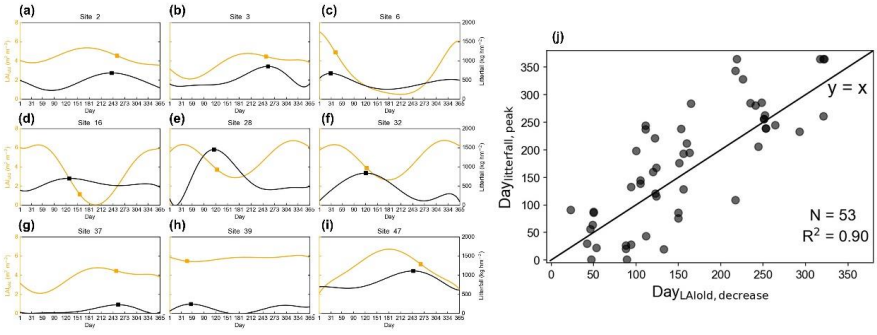

Figure 12. Evaluation of simulated LAI_{old} using site-observed litterfall seasonality. (a-i) Days of a sharping decrease in LAI_{old} in comparison with days of corresponding litterfall peak at 9 specific sites for examples. (j) Comparisons of the days when LAI_{old} decreases sharpest (Day_{LAIold}) against the days when monthly litterfall peaks ($Day_{litterfall}$).

4 Discussion

Leaf age-dependent LAI performs well in describing the seasonal replacements of canopy leaves in TEFs (Wu et al., 2016; Chen et al., 2020), showing to be a critical plant trait for representing the tropical and subtropical phenology (Doughty and

https://doi.org/10.5194/essd-2022-436
Preprint. Discussion started: 17 January 2023

Goulden, 2008b; Saleska et al., 2007). However, to our knowledge, there are currently no continental-scale information of such leaf age-dependent LAI data over the whole TEFs, as it can neither be mapped from sparse site observations (Wu et al., 2016), nor be modeled from ESMs which were triggered by unclear climatic drivers (Chen et al., 2020). These hinder global researches on accurately simulations of large-scale photosynthesis (GPP) seasonality using remote sensing approaches and ESMs (Chen et al., 2020).

The Lad-LAI product developed in this study is a new continental-scale grid dataset of monthly LAI in different leaf age cohorts. Although lacking of enough *in situ* observations for adequate validations, the seasonality of three LAI cohorts performs well at the three sites (K67, K34 and Din) with very fine collections of monthly LAI_{young}, LAI_{mature}, and LAI_{old}. To test the robustness of the grid Lad-LAI products over the whole TEFs, the seasonality of LAI_{mature} seasonality was also validated pixel by pixel using satellite-based EVI products and the phase of LAI_{old} seasonality were compared with the those of seasonal litterfall data from 53 site measurements, respectively. Moreover, the $LAI_{young+mature}$ from the new Lad-LAI products can also directly represent the large-scale dry-season green-up of canopy leaves north of the Equator. Therefore, direct and indirect evaluations both demonstrated the robustness of the new grid Lad-LAI products.

It should be noted that, over the regions with large magnitude of annual precipitation nearby the Equator, there is no obvious dry seasons and thus tree canopy phenology changes smaller than higher-latitude ones throughout the year (Yang et al., 2021). Thus, the accuracy in the seasonality of LAI cohorts depend highly on that of input SIF data, which shows marginally small seasonal changes nearby the equator. Our analyses showed that the $LAI_{young+mature}$ cohorts from Lad-LAI succeed to capture the bimodal phenology of TEFs nearby the equator. It is also worth noting that we use a constant to calculate to transfer from SIF data to GPP and also assume a constant value for the total LAI over the whole TEFs, which tend to bring unexpected errors in the

https://doi.org/10.5194/essd-2022-436
Preprint. Discussion started: 17 January 2023

magnitudes of simulated LAI cohorts. This can be seen from the MSD evaluations, where the bias-related term dominated the total MSD, especially in regions nearby the Equator. However, this bring less impacts on the seasonality of Lad-LAI, as the phase-related term of MSD is much smaller.

Additionally, the maximum carboxylation rate ($V_{c,max}$) of leaves changes significantly with leaf age (Xu et al., 2017). Currently, most Earth system models (ESMs) define $V_{c,max}$ as a function of leaf age whereas their relationship is still less well understood in TEFs due to sparse in-situ measurements (Chen et al., 2020). This may consequentially lead to poorly representation of LAI and GPP seasonality in ESMs (De Weirdt et al., 2012). To overcome this challenge, we simplified the tree canopy into three big leaves (i.e., young, mature and old) in TEFs, similar as the two-big leaves model developed for temperate and boreal forests (Best et al., 2011; Clark et al., 2011; Harper et al., 2016), which simplified tree canopy into sun and shade leaves. However, some uncertain remains on the assumption, as it neglected the spatial and temporal variations of $V_{c,max}$, which also changes with seasonal climate anomaly and also differs between nearby pixels in high heterogeneous forest ecosystems. These may bring uncertainties for simulating seasonal An and therefore influence the seasonality of Lad-LAI.

In summary, this study developed a new method to produce the first grid dataset of leaf age-dependent LAI product over the continental scale. Although some uncertainties remain associated with this assumption, it is important to improve the GPP simulation accuracy in most ESMs that are currently run at a coarser resolution. And, the proposed method could provide simulations of accurate age-dependent LAI seasonality by dividing canopy leaves into more age cohorts. With the development of remote sensing technology, finer temporal and spatial resolutions of SIF products will also enable finer temporal and spatial resolutions maps of Lad-LAI products.

5. Data availability

https://doi.org/10.5194/essd-2022-436
Preprint. Discussion started: 17 January 2023

The 0.25 degree leaf age-dependent LAI seasonality (Lad-LAI) datasets from 2001-2018 presented in this paper are available at https://doi.org/10.6084/m9.figshare.21700955.v2 (Yang et al., 2022). The format of this dataset is GeoTiff, with a spatial reference of WGS84. Each file in this dataset is named based on leaf age, start year, end year, and monthly. We divided the LAI into three cohorts: LAI_{young}, LAI_{mature}, and LAI_{old}.

6. Conclusion

This study for the first-time mapped continental-scale grid dataset of monthly LAI in three leaf age cohorts from 2001-2018 RTSIF data. The LAI seasonality of young, mature and old leaves was evaluated using *in situ* measurements of seasonal LAI data, satellite based EVI and *in situ* measurements of seasonal litterfall data. The evaluations from these independent datasets all demonstrate the robustness of the seasonality of three leaf age cohorts. The new Lad-LAI products indicate diverse patterns over the whole tropical and subtropical regions. In central and south Amazon, LAI_{young} and LAI_{mature} decrease at early wet season around February and convert to increase at early wet season around June. On the contrary, in subtropical Asia, LAI_{young} and LAI_{mature} increase during the wet season and peak with largest rainfall at June or July. In regions nearby the Equator, the LAI cohorts show a bimodal phenology but with marginally small changes in magnitudes. The proposed method will enable to produce finer temporal and spatial resolutions maps of Lad-LAI products by using precise temporal and spatial resolutions data as the inputs. The Lad-LAI products will be help for diagnosing the adaption of tropical and subtropical forest to climate change; and will also help improve the development of phenology models in ESMs.

Supplement. The supplement related to this article will be available online at once accepted.

https://doi.org/10.5194/essd-2022-436
Preprint. Discussion started: 17 January 2023

Author contributions. XZ designed the research and wrote the paper. XY performed the analyses. All the authors edited and revised the paper.

Competing interests. The authors declare no competing interests.

Financial support.

This study was supported by the National Natural Science Foundation of China (grant numbers 31971458, 41971275), the Guangdong Major Project of Basic and Applied Basic Research (grant number 2020B0301030004), the Special high-level plan project of Guangdong Province (grant number 2016TQ03Z354), Innovation Group Project of Southern Marine Science and Engineering Guangdong Laboratory (Zhuhai) (grant number 311021009).

Acknowledgement

Thanks for Dr. Jin Wu from Hongkong University for providing the observation data of LAI cohorts at K67 and K34 sites in Amazon. We would also like to thank the editor and reviewers for their valuable time in reviewing the manuscript.

Reference:

Albert, L. P., Wu, J., Prohaska, N., de Camargo, P. B., Huxman, T. E., Tribuzy, E. S., Ivanov, V. Y., Oliveira, R. S., Garcia, S., Smith, M. N., Oliveira Junior, R. C., Restrepo-Coupe, N., da Silva, R., Stark, S. C., Martins, G. A., Penha, D. V., and Saleska, S. R.: Age-dependent leaf physiology and consequences for crown-scale carbon uptake during the dry season in an Amazon evergreen forest, New Phytol, 219, 870-884, 10.1111/nph.15056, 2018.

Anber, U., Gentine, P., Wang, S., and Sobel, A. H.: Fog and rain in the Amazon, Proc Natl Acad Sci U S A, 112, 11473-11477, 10.1073/pnas.1505077112, 2015.

Aragao, L. E., Poulter, B., Barlow, J. B., Anderson, L. O., Malhi, Y., Saatchi, S., Phillips, O. L., and Gloor, E.: Environmental change and the carbon balance of Amazonian forests, Biol Rev Camb Philos Soc, 89, 913-931, 10.1111/brv.12088, 2014.

Araújo, A. C.: Comparative measurements of carbon dioxide fluxes from two nearby towers in a central Amazonian rainforest: The Manaus LBA site, Journal of Geophysical Research, 107, 10.1029/2001jd000676, 2002.

https://doi.org/10.5194/essd-2022-436
Preprint. Discussion started: 17 January 2023

Arora, V. K. and Boer, G. J.: Fire as an interactive component of dynamic vegetation models, Journal of Geophysical Research: Biogeosciences, 110, n/a-n/a, 10.1029/2005jg000042, 2005.

Barlow, J., Gardner, T. A., Ferreira, L. V., and Peres, C. A.: Litter fall and decomposition in primary, secondary and plantation forests in the Brazilian Amazon, Forest Ecology and Management, 247, 91-97, 10.1016/j.foreco.2007.04.017, 2007.

Beer, C., Reichstein, M., Tomelleri, E., Ciais, P., Jung, M., Carvalhais, N., Rodenbeck, C., Arain, M. A., Baldocchi, D., Bonan, G. B., Bondeau, A., Cescatti, A., Lasslop, G., Lindroth, A., Lomas, M., Luyssaert, S., Margolis, H., Oleson, K. W., Roupsard, O., Veenendaal, E., Viovy, N., Williams, C., Woodward, F. I., and Papale, D.: Terrestrial gross carbon dioxide uptake: global distribution and covariation with climate, Science, 329, 834-838, 10.1126/science.1184984, 2010.

Bernacchi, C. J., Pimentel, C., and Long, S. P.: In vivo temperature response functions of parameters required to model RuBP-limited photosynthesis, Plant, Cell & Environment, 26, 1419-1430, 10.1046/j.0016-8025.2003.01050.x, 2003.

Bernacchi, C. J., Bagley, J. E., Serbin, S. P., Ruiz-Vera, U. M., Rosenthal, D. M., and Vanloocke, A.: Modelling C(3) photosynthesis from the chloroplast to the ecosystem, Plant Cell Environ, 36, 1641-1657, 10.1111/pce.12118, 2013.

Best, M. J., Pryor, M., Clark, D. B., Rooney, G. G., Essery, R. L. H., Ménard, C. B., Edwards, J. M., Hendry, M. A., Porson, A., Gedney, N., Mercado, L. M., Sitch, S., Blyth, E., Boucher, O., Cox, P. M., Grimmond, C. S. B., and Harding, R. J.: The Joint UK Land Environment Simulator (JULES), model description–Part 1: Energy and water fluxes. Geoscientific Model Development, 4, 677–699, 2011.

Chen, J., Wang, R., Liu, Y., He, L., Croft, H., Luo, X., Wang, H., Smith, N. G., Keenan, T. F., Prentice, I. C., Zhang, Y., Ju, W., Dong, N.: Global datasets of leaf photosynthetic capacity for ecological and earth system research, Earth Syst. Sci. Data, 14(9), 4077-4093, 10.5194/essd-14-4077-2022, 2022.

Chen, X., Huang, Y., Nie, C., Zhang, S., Wang, G., Chen, S., and Chen, Z.: A long-term reconstructed TROPOMI solar-induced fluorescence dataset using machine learning algorithms, Sci Data, 9, 427, 10.1038/s41597-022-01520-1, 2022.

Chen, X., Maignan, F., Viovy, N., Bastos, A., Goll, D., Wu, J., Liu, L., Yue, C., Peng, S., Yuan, W., Conceição, A. C., O'Sullivan, M., and Ciais, P.: Novel Representation of Leaf Phenology Improves Simulation of Amazonian Evergreen Forest Photosynthesis in a Land Surface Model, Journal of Advances in Modeling Earth Systems, 12, 10.1029/2018ms001565, 2020.

Chen, X., Ciais, P., Maignan, F., Zhang, Y., Bastos, A., Liu, L., Bacour, C., Fan, L., Gentine, P., Goll, D., Green, J., Kim, H., Li, L., Liu, Y., Peng, S., Tang, H., Viovy, N., Wigneron, J. P., Wu, J., Yuan, W., and Zhang, H.: Vapor Pressure Deficit and

https://doi.org/10.5194/essd-2022-436
Preprint. Discussion started: 17 January 2023

Sunlight Explain Seasonality of Leaf Phenology and Photosynthesis Across Amazonian Evergreen Broadleaved Forest, Global Biogeochemical Cycles, 35, 10.1029/2020gb006893, 2021.

Clark, D. B., Mercado, L. M., Sitch, S., Jones, C. D., Gedney, N., Best, M. J., Pryor, M., Rooney, G. G., Essery, R. L. H., Blyth, E., Boucher, O., Harding, R. J., Huntingford, C., and Cox, P. M.: The Joint UK Land Environment Simulator (JULES), model description–Part 2: Carbon fluxes and vegetation dynamics. Geoscientific Model Development, 4, 701–722, 2011.

Cramer, W., Bondeau, A., Woodward, F. I., Prentice, I. C., Betts, R. A., Brovkin, V., Cox, P. M., Fisher, V., Foley, J. A., Friend, A. D., Kucharik, C., Lomas, M. R., Ramankutty, N., Sitch, S., Smith, B., White, A., and Young-Molling, C.: Global response of terrestrial ecosystem structure and function to CO2 and climate change: results from six dynamic global vegetation models, Global Change Biology, 7, 357-373, 10.1046/j.1365-2486.2001.00383.x, 2001.

Dantas, M. and Phillipson, J.: Litterfall and litter nutrient content in primary and secondary Amazonian 'terra firme' rain forest, Journal of Tropical Ecology, 5, 27-36, 10.1017/s0266467400003199, 1989.

de Moura, Y. M., Galvão, L. S., Hilker, T., Wu, J., Saleska, S., do Amaral, C. H., Nelson, B. W., Lopes, A. P., Wiedeman, K. K., Prohaska, N., de Oliveira, R. C., Machado, C. B., and Aragão, L. E. O. C.: Spectral analysis of amazon canopy phenology during the dry season using a tower hyperspectral camera and modis observations, ISPRS Journal of Photogrammetry and Remote Sensing, 131, 52-64, 10.1016/j.isprsjprs.2017.07.006, 2017.

De Weirdt, M., Verbeeck, H., Maignan, F., Peylin, P., Poulter, B., Bonal, D., Ciais, P., and Steppe, K.: Seasonal leaf dynamics for tropical evergreen forests in a process-based global ecosystem model, Geoscientific Model Development, 5, 1091-1108, 10.5194/gmd-5-1091-2012, 2012.

Dechant, B., Ryu, Y., Badgley, G., Zeng, Y., Berry, J. A., Zhang, Y., Goulas, Y., Li, Z., Zhang, Q., Kang, M., Li, J., and Moya, I.: Canopy structure explains the relationship between photosynthesis and sun-induced chlorophyll fluorescence in crops, Remote Sensing of Environment, 241, 10.1016/j.rse.2020.111733, 2020.

Dee, D. P., Uppala, S. M., Simmons, A. J., Berrisford, P., Poli, P., Kobayashi, S., Andrae, U., Balmaseda, M. A., Balsamo, G., Bauer, P., Bechtold, P., Beljaars, A. C. M., van de Berg, L., Bidlot, J., Bormann, N., Delsol, C., Dragani, R., Fuentes, M., Geer, A. J., Haimberger, L., Healy, S. B., Hersbach, H., Hólm, E. V., Isaksen, L., Kållberg, P., Köhler, M., Matricardi, M., McNally, A. P., Monge-Sanz, B. M., Morcrette, J. J., Park, B. K., Peubey, C., de Rosnay, P., Tavolato, C., Thépaut, J. N., and Vitart, F.: The ERA-Interim reanalysis: configuration and performance of the data assimilation system, Quarterly Journal of the Royal Meteorological Society, 137, 553-597, 10.1002/qj.828, 2011.

Doughty, C. E. and Goulden, M. L.: Are tropical forests near a high temperature threshold?, Journal of Geophysical Research: Biogeosciences, 113, n/a-n/a,

10.1029/2007jg000632, 2008a.

Doughty, C. E. and Goulden, M. L.: Seasonal patterns of tropical forest leaf area index and CO2exchange, Journal of Geophysical Research: Biogeosciences, 113, n/a-n/a, 10.1029/2007jg000590, 2008b.

Doughty, C. E., Metcalfe, D. B., Girardin, C. A., Amezquita, F. F., Cabrera, D. G., Huasco, W. H., Silva-Espejo, J. E., Araujo-Murakami, A., da Costa, M. C., Rocha, W., Feldpausch, T. R., Mendoza, A. L., da Costa, A. C., Meir, P., Phillips, O. L., and Malhi, Y.: Drought impact on forest carbon dynamics and fluxes in Amazonia, Nature, 519, 78-82, 10.1038/nature14213, 2015.

Farquhar, G. D., von Caemmerer, S., and Berry, J. A.: A biochemical model of photosynthetic CO2 assimilation in leaves of C 3 species, Planta, 149, 78-90, 10.1007/BF00386231, 1980.

Gonçalves, N. B., Lopes, A. P., Dalagnol, R., Wu, J., Pinho, D. M., and Nelson, B. W.: Both near-surface and satellite remote sensing confirm drought legacy effect on tropical forest leaf phenology after 2015/2016 ENSO drought, Remote Sensing of Environment, 237, 10.1016/j.rse.2019.111489, 2020.

Guan, K., Pan, M., Li, H., Wolf, A., Wu, J., Medvigy, D., Caylor, K. K., Sheffield, J., Wood, E. F., Malhi, Y., Liang, M., Kimball, J. S., Saleska, Scott R., Berry, J., Joiner, J., and Lyapustin, A. I.: Photosynthetic seasonality of global tropical forests constrained by hydroclimate, Nature Geoscience, 8, 284-289, 10.1038/ngeo2382, 2015.

Harper, A., Cox, P., Friedlingstein, P., Wiltshire, A. J., Jones, C. D., Sitch, S., . . . van Bodegom, P.: Improved representation of plant functional types and physiology in the Joint UK Land Environment Simulator (JULES v4.2) using plant trait information. Geoscientific Model Development Discussions, 9, 2415–2440, 2016.

Huete, A., Didan, K., Miura, T., Rodriguez, E. P., Gao, X., and Ferreira, L. G.: Overview of the radiometric and biophysical performance of the MODIS vegetation indices, Remote Sensing of Environment, 83, 195-213, 10.1016/s0034-4257(02)00096-2, 2002.

Huete, A. R., Didan, K., Shimabukuro, Y. E., Ratana, P., Saleska, S. R., Hutyra, L. R., Yang, W., Nemani, R. R., and Myneni, R.: Amazon rainforests green-up with sunlight in dry season, Geophysical Research Letters, 33, 10.1029/2005gl025583, 2006.

June, T., Evans, J. R., and Farquhar, G. D.: A simple new equation for the reversible temperature dependence of photosynthetic electron transport: a study on soybean leaf, Funct Plant Biol, 31, 275-283, 10.1071/FP03250, 2004.

Kartikeyan, B., Sarkar, A., and Majumder, K. L.: A segmentation approach to classification of remote sensing imagery, International Journal of Remote Sensing, 19, 1695-1709, 1998.

Keller, M., Palace, M., and Hurtt, G.: Biomass estimation in the Tapajos National Forest, Brazil, Forest Ecology and Management, 154, 371-382, 10.1016/s0378-1127(01)00509-6, 2001.

Kobayashi, K. and Salam, M. U.: Comparing Simulated and Measured Values Using Mean Squared Deviation and its Components, Agronomy Journal, 92, 10.1007/s100870050043, 2000.

Li, Q., Chen, X., Yuan, W., Lu, H., Shen, R., Wu, S., Gong, F., Dai, Y., Liu, L., Sun, Q., Zhang, C., and Su, Y.: Remote Sensing of Seasonal Climatic Constraints on Leaf Phenology Across Pantropical Evergreen Forest Biome, Earth's Future, 9, 10.1029/2021ef002160, 2021.

Lin, Y.-S., Medlyn, B. E., Duursma, R. A., Prentice, I. C., Wang, H., Baig, S., Eamus, D., de Dios, Victor R., Mitchell, P., Ellsworth, D. S., de Beeck, M. O., Wallin, G., Uddling, J., Tarvainen, L., Linderson, M.-L., Cernusak, L. A., Nippert, J. B., Ocheltree, T. W., Tissue, D. T., Martin-StPaul, N. K., Rogers, A., Warren, J. M., De Angelis, P., Hikosaka, K., Han, Q., Onoda, Y., Gimeno, T. E., Barton, C. V. M., Bennie, J., Bonal, D., Bosc, A., Löw, M., Macinins-Ng, C., Rey, A., Rowland, L., Setterfield, S. A., Tausz-Posch, S., Zaragoza-Castells, J., Broadmeadow, M. S. J., Drake, J. E., Freeman, M., Ghannoum, O., Hutley, Lindsay B., Kelly, J. W., Kikuzawa, K., Kolari, P., Koyama, K., Limousin, J.-M., Meir, P., Lola da Costa, A. C., Mikkelsen, T. N., Salinas, N., Sun, W., and Wingate, L.: Optimal stomatal behaviour around the world, Nature Climate Change, 5, 459-464, 10.1038/nclimate2550, 2015.

Lopes, A. P., Nelson, B. W., Wu, J., Graça, P. M. L. d. A., Tavares, J. V., Prohaska, N., Martins, G. A., and Saleska, S. R.: Leaf flush drives dry season green-up of the Central Amazon, Remote Sensing of Environment, 182, 90-98, 10.1016/j.rse.2016.05.009, 2016.

Maes, W. H., Gentine, P., Verhoest, N. E. C., and Miralles, D. G.: Potential evaporation at eddy-covariance sites across the globe, Hydrology and Earth System Sciences, 23, 925-948, 10.5194/hess-23-925-2019, 2019.

Manoli, G., Ivanov, V. Y., and Fatichi, S.: Dry-Season Greening and Water Stress in Amazonia: The Role of Modeling Leaf Phenology, Journal of Geophysical Research: Biogeosciences, 123, 1909-1926, 10.1029/2017jg004282, 2018.

Medlyn, B. E., Duursma, R. A., Eamus, D., Ellsworth, D. S., Prentice, I. C., Barton, C. V. M., Crous, K. Y., De Angelis, P., Freeman, M., and Wingate, L.: Reconciling the optimal and empirical approaches to modelling stomatal conductance, Global Change Biology, 17, 2134-2144, 10.1111/j.1365-2486.2010.02375.x, 2011.

Merkl, R. and Waack, S.: Bioinformatik interaktiv, John Wiley & Sons, 2009.

Midoko Iponga, D., Mpikou, R. G. J., Loumeto, J., and Picard, N.: The effect of different anthropogenic disturbances on litterfall of a dominant pioneer rain forest tree in Gabon, African Journal of Ecology, 58, 281-290, 10.1111/aje.12696, 2019.

Morton, D. C., Nagol, J., Carabajal, C. C., Rosette, J., Palace, M., Cook, B. D., Vermote, E. F., Harding, D. J., and North, P. R.: Amazon forests maintain consistent canopy structure and greenness during the dry season, Nature, 506, 221-224, 10.1038/nature13006, 2014.

Ndakara, O. E.: Litterfall and Nutrient Returns in Isolated Stands of <i>Persea

https://doi.org/10.5194/essd-2022-436
Preprint. Discussion started: 17 January 2023

gratissima</i> (Avocado Pear) in the Rainforest Zone of Southern Nigeria, Ethiopian Journal of Environmental Studies and Management, 4, 10.4314/ejesm.v4i3.6, 2011.

Pastorello, G., Trotta, C., Canfora, E., Chu, H., Christianson, D., Cheah, Y. W., Poindexter, C., Chen, J., Elbashandy, A., Humphrey, M., Isaac, P., Polidori, D., Reichstein, M., Ribeca, A., van Ingen, C., Vuichard, N., Zhang, L., Amiro, B., Ammann, C., Arain, M. A., Ardo, J., Arkebauer, T., Arndt, S. K., Arriga, N., Aubinet, M., Aurela, M., Baldocchi, D., Barr, A., Beamesderfer, E., Marchesini, L. B., Bergeron, O., Beringer, J., Bernhofer, C., Berveiller, D., Billesbach, D., Black, T. A., Blanken, P. D., Bohrer, G., Boike, J., Bolstad, P. V., Bonal, D., Bonnefond, J. M., Bowling, D. R., Bracho, R., Brodeur, J., Brummer, C., Buchmann, N., Burban, B., Burns, S. P., Buysse, P., Cale, P., Cavagna, M., Cellier, P., Chen, S., Chini, I., Christensen, T. R., Cleverly, J., Collalti, A., Consalvo, C., Cook, B. D., Cook, D., Coursolle, C., Cremonese, E., Curtis, P. S., D'Andrea, E., da Rocha, H., Dai, X., Davis, K. J., Cinti, B., Grandcourt, A., Ligne, A., De Oliveira, R. C., Delpierre, N., Desai, A. R., Di Bella, C. M., Tommasi, P. D., Dolman, H., Domingo, F., Dong, G., Dore, S., Duce, P., Dufrene, E., Dunn, A., Dusek, J., Eamus, D., Eichelmann, U., ElKhidir, H. A. M., Eugster, W., Ewenz, C. M., Ewers, B., Famulari, D., Fares, S., Feigenwinter, I., Feitz, A., Fensholt, R., Filippa, G., Fischer, M., Frank, J., Galvagno, M., Gharun, M., Gianelle, D., Gielen, B., Gioli, B., Gitelson, A., Goded, I., Goeckede, M., Goldstein, A. H., Gough, C. M., Goulden, M. L., Graf, A., Griebel, A., Gruening, C., Grunwald, T., Hammerle, A., Han, S., Han, X., Hansen, B. U., Hanson, C., Hatakka, J., He, Y., Hehn, M., Heinesch, B., Hinko-Najera, N., Hortnagl, L., Hutley, L., Ibrom, A., Ikawa, H., Jackowicz-Korczynski, M., Janous, D., Jans, W., Jassal, R., Jiang, S., Kato, T., Khomik, M., Klatt, J., Knohl, A., Knox, S., Kobayashi, H., Koerber, G., Kolle, O., Kosugi, Y., Kotani, A., Kowalski, A., Kruijt, B., Kurbatova, J., Kutsch, W. L., Kwon, H., Launiainen, S., Laurila, T., Law, B., Leuning, R., Li, Y., Liddell, M., Limousin, J. M., Lion, M., Liska, A. J., Lohila, A., Lopez-Ballesteros, A., Lopez-Blanco, E., Loubet, B., Loustau, D., Lucas-Moffat, A., Luers, J., Ma, S., Macfarlane, C., Magliulo, V., Maier, R., Mammarella, I., Manca, G., Marcolla, B., Margolis, H. A., Marras, S., Massman, W., Mastepanov, M., Matamala, R., Matthes, J. H., Mazzenga, F., McCaughey, H., McHugh, I., McMillan, A. M. S., Merbold, L., Meyer, W., Meyers, T., Miller, S. D., Minerbi, S., Moderow, U., Monson, R. K., Montagnani, L., Moore, C. E., Moors, E., Moreaux, V., Moureaux, C., Munger, J. W., Nakai, T., Neirynck, J., Nesic, Z., Nicolini, G., Noormets, A., Northwood, M., Nosetto, M., Nouvellon, Y., Novick, K., Oechel, W., Olesen, J. E., Ourcival, J. M., Papuga, S. A., Parmentier, F. J., Paul-Limoges, E., Pavelka, M., Peichl, M., Pendall, E., Phillips, R. P., Pilegaard, K., Pirk, N., Posse, G., Powell, T., Prasse, H., Prober, S. M., Rambal, S., Rannik, U., Raz-Yaseef, N., Rebmann, C., Reed, D., Dios, V. R., Restrepo-Coupe, N., Reverter, B. R., Roland, M., Sabbatini, S., Sachs, T., Saleska, S. R., Sanchez-Canete, E. P., Sanchez-Mejia, Z.

https://doi.org/10.5194/essd-2022-436
Preprint. Discussion started: 17 January 2023

M., Schmid, H. P., Schmidt, M., Schneider, K., Schrader, F., Schroder, I., Scott, R. L., Sedlak, P., Serrano-Ortiz, P., Shao, C., Shi, P., Shironya, I., Siebicke, L., Sigut, L., Silberstein, R., Sirca, C., Spano, D., Steinbrecher, R., Stevens, R. M., Sturtevant, C., Suyker, A., Tagesson, T., Takanashi, S., Tang, Y., Tapper, N., Thom, J., Tomassucci, M., Tuovinen, J. P., Urbanski, S., Valentini, R., van der Molen, M., van Gorsel, E., van Huissteden, K., Varlagin, A., Verfaillie, J., Vesala, T., Vincke, C., Vitale, D., Vygodskaya, N., Walker, J. P., Walter-Shea, E., Wang, H., Weber, R., Westermann, S., Wille, C., Wofsy, S., Wohlfahrt, G., Wolf, S., Woodgate, W., Li, Y., Zampedri, R., Zhang, J., Zhou, G., Zona, D., Agarwal, D., Biraud, S., Torn, M., and Papale, D.: The FLUXNET2015 dataset and the ONEFlux processing pipeline for eddy covariance data, Sci Data, 7, 225, 10.1038/s41597-020-0534-3, 2020.

Pearson, K.: VII. Mathematical contributions to the theory of evolution.—III. Regression, heredity, and panmixia, Philosophical Transactions of the Royal Society of London. Series A, Containing Papers of a Mathematical or Physical Character, 187, 253-318, 10.1098/rsta.1896.0007, 1896.

Piao, S., Liu, Q., Chen, A., Janssens, I. A., Fu, Y., Dai, J., Liu, L., Lian, X., Shen, M., and Zhu, X.: Plant phenology and global climate change: Current progresses and challenges, Glob Chang Biol, 25, 1922-1940, 10.1111/gcb.14619, 2019.

Restrepo-Coupe, N., Levine, N. M., Christoffersen, B. O., Albert, L. P., Wu, J., Costa, M. H., Galbraith, D., Imbuzeiro, H., Martins, G., da Araujo, A. C., Malhi, Y. S., Zeng, X., Moorcroft, P., and Saleska, S. R.: Do dynamic global vegetation models capture the seasonality of carbon fluxes in the Amazon basin? A data-model intercomparison, Glob Chang Biol, 23, 191-208, 10.1111/gcb.13442, 2017.

Restrepo-Coupe, N., da Rocha, H. R., Hutyra, L. R., da Araujo, A. C., Borma, L. S., Christoffersen, B., Cabral, O. M. R., de Camargo, P. B., Cardoso, F. L., da Costa, A. C. L., Fitzjarrald, D. R., Goulden, M. L., Kruijt, B., Maia, J. M. F., Malhi, Y. S., Manzi, A. O., Miller, S. D., Nobre, A. D., von Randow, C., Sá, L. D. A., Sakai, R. K., Tota, J., Wofsy, S. C., Zanchi, F. B., and Saleska, S. R.: What drives the seasonality of photosynthesis across the Amazon basin? A cross-site analysis of eddy flux tower measurements from the Brasil flux network, Agricultural and Forest Meteorology, 182-183, 128-144, 10.1016/j.agrformet.2013.04.031, 2013.

Ryu, Y., Baldocchi, D. D., Kobayashi, H., van Ingen, C., Li, J., Black, T. A., Beringer, J., van Gorsel, E., Knohl, A., Law, B. E., and Roupsard, O.: Integration of MODIS land and atmosphere products with a coupled-process model to estimate gross primary productivity and evapotranspiration from 1 km to global scales, Global Biogeochemical Cycles, 25, n/a-n/a, 10.1029/2011gb004053, 2011.

Saatchi, S. S., Harris, N. L., Brown, S., Lefsky, M., Mitchard, E. T., Salas, W., Zutta, B. R., Buermann, W., Lewis, S. L., Hagen, S., Petrova, S., White, L., Silman, M., and Morel, A.: Benchmark map of forest carbon stocks in tropical regions across three continents, Proc Natl Acad Sci U S A, 108, 9899-9904, 10.1073/pnas.1019576108, 2011.

Saleska, S. R., Didan, K., Huete, A. R., and da Rocha, H. R.: Amazon forests green-up

https://doi.org/10.5194/essd-2022-436
Preprint. Discussion started: 17 January 2023

during 2005 drought, Science, 318, 612, 10.1126/science.1146663, 2007.

Saleska, S. R., Wu, J., Guan, K., Araujo, A. C., Huete, A., Nobre, A. D., and Restrepo-Coupe, N.: Dry-season greening of Amazon forests, Nature, 531, E4-5, 10.1038/nature16457, 2016.

Saleska, S. R., Miller, S. D., Matross, D. M., Goulden, M. L., Wofsy, S. C., da Rocha, H. R., de Camargo, P. B., Crill, P., Daube, B. C., de Freitas, H. C., Hutyra, L., Keller, M., Kirchhoff, V., Menton, M., Munger, J. W., Pyle, E. H., Rice, A. H., and Silva, H.: Carbon in Amazon forests: unexpected seasonal fluxes and disturbance-induced losses, Science, 302, 1554-1557, 10.1126/science.1091165, 2003.

Wang, C., Li, J., Liu, Q., Zhong, B., Wu, S., and Xia, C.: Analysis of Differences in Phenology Extracted from the Enhanced Vegetation Index and the Leaf Area Index, Sensors (Basel), 17, 10.3390/s17091982, 2017.

Weiss, A. and Norman, J. M.: Partitioning solar radiation into direct and diffuse, visible and near-infrared components, Agricultural and Forest Meteorology, 34, 205-213, 10.1016/0168-1923(85)90020-6, 1985.

Wu, J., Serbin, S. P., Xu, X., Albert, L. P., Chen, M., Meng, R., Saleska, S. R., and Rogers, A.: The phenology of leaf quality and its within-canopy variation is essential for accurate modeling of photosynthesis in tropical evergreen forests, Glob Chang Biol, 23, 4814-4827, 10.1111/gcb.13725, 2017.

Wu, J., Kobayashi, H., Stark, S. C., Meng, R., Guan, K., Tran, N. N., Gao, S., Yang, W., Restrepo-Coupe, N., Miura, T., Oliviera, R. C., Rogers, A., Dye, D. G., Nelson, B. W., Serbin, S. P., Huete, A. R., and Saleska, S. R.: Biological processes dominate seasonality of remotely sensed canopy greenness in an Amazon evergreen forest, New Phytol, 217, 1507-1520, 10.1111/nph.14939, 2018.

Wu, J., Albert, L. P., Lopes, A. P., Restrepo-Coupe, N., Hayek, M., Wiedemann, K. T., Guan, K., Stark, S. C., Christoffersen, B., Prohaska, N., Tavares, J. V., Marostica, S., Kobayashi, H., Ferreira, M. L., Campos, K. S., da Silva, R., Brando, P. M., Dye, D. G., Huxman, T. E., Huete, A. R., Nelson, B. W., and Saleska, S. R.: Leaf development and demography explain photosynthetic seasonality in Amazon evergreen forests, Science, 351, 972-976, 10.1126/science.aad5068, 2016.

Xiao, X., Zhang, Q., Saleska, S., Hutyra, L., De Camargo, P., Wofsy, S., Frolking, S., Boles, S., Keller, M., and Moore, B.: Satellite-based modeling of gross primary production in a seasonally moist tropical evergreen forest, Remote Sensing of Environment, 94, 105-122, 10.1016/j.rse.2004.08.015, 2005.

Xu, L., Saatchi, S. S., Yang, Y., Myneni, R. B., Frankenberg, C., Chowdhury, D., and Bi, J.: Satellite observation of tropical forest seasonality: spatial patterns of carbon exchange in Amazonia, Environmental Research Letters, 10, 10.1088/1748-9326/10/8/084005, 2015.

Xu, X., Medvigy, D., Joseph Wright, S., Kitajima, K., Wu, J., Albert, L. P., Martins, G. A., Saleska, S. R., and Pacala, S. W.: Variations of leaf longevity in tropical moist forests predicted by a trait-driven carbon optimality model, Ecol Lett, 20, 1097-1106, 10.1111/ele.12804, 2017.

https://doi.org/10.5194/essd-2022-436
Preprint. Discussion started: 17 January 2023

Yang, X., Tang, J., Mustard, J. F., Lee, J.-E., Rossini, M., Joiner, J., Munger, J. W., Kornfeld, A., and Richardson, A. D.: Solar-induced chlorophyll fluorescence that correlates with canopy photosynthesis on diurnal and seasonal scales in a temperate deciduous forest, Geophysical Research Letters, 42, 2977-2987, 10.1002/2015gl063201, 2015.

Yang, X., Wu, J., Chen, X., Ciais, P., Maignan, F., Yuan, W., Piao, S., Yang, S., Gong, F., Su, Y., Dai, Y., Liu, L., Zhang, H., Bonal, D., Liu, H., Chen, G., Lu, H., Wu, S., Fan, L., Gentine, P., and Wright, S. J.: A comprehensive framework for seasonal controls of leaf abscission and productivity in evergreen broadleaved tropical and subtropical forests, Innovation (Camb), 2, 100154, 10.1016/j.xinn.2021.100154, 2021.

Yang, X., Chen, X., Ren, J., Yuan, W., Liu, L., Liu, J., Chen, D., Xiao, Y., Wu, S., Fan, L., Dai, X., Su, Y.: Leaf age-dependent LAI seasonality product (Lad-LAI) over tropical and subtropical evergreen broadleaved forests. figshare. Dataset. https://doi.org/10.6084/m9.figshare.21700955.v2. 2022.

Yuan, W., Zheng, Y., Piao, S., Ciais, P., Lombardozzi, D., Wang, Y., Ryu, Y., Chen, G., Dong, W., Hu, Z., Jain, A. K., Jiang, C., Kato, E., Li, S., Lienert, S., Liu, S., Nabel, J., Qin, Z., Quine, T., Sitch, S., Smith, W. K., Wang, F., Wu, C., Xiao, Z., and Yang, S.: Increased atmospheric vapor pressure deficit reduces global vegetation growth, Sci Adv, 5, eaax1396, 10.1126/sciadv.aax1396, 2019.